APPLICATION OF CHARGE-COUPLED DEVICES TO INFRARED DETECTION AND IMAGING

A. J. Steckl*, R. D. Nelson*, B. T. French* and D. Schechter**

ABSTRACT. A review of infrared sensitive charge-coupled devices is presented. Operational requirements of typical IRCCD applications are briefly introduced. IRCCD devices are divided into two major categories: (a) monolithic devices, which essentially extend the original CCD concept into the IR. Monolithic IRCCD's discussed include inversion-mode devices (with narrow bandgap semiconductor substrate), accumulation-mode devices (extrinsic wide bandgap semiconductor substrate) and Schottky barrier devices (internal photoemission). (b) Hybrid devices, in which the function of detection and signal processing are performed in separate but integratable components by an array of IR detectors and a silicon CCD shift register unit. Hybrid IRCCD's discussed include both direct injection devices (in conjunction with photovoltaic IR detectors) and indirect injection devices (in conjunction with pyroelectric and photoconductive devices).

I. INTRODUCTION

Since the invention of charge-coupled devices by Boyle and Smith (ref 1) in 1970, the remarkable versatility of this class of devices has lead to their application in a diverse number of fields. These applications include visible light imagers (e.g. TV cameras, optical character reader), digital and semianalog memories, communications and signal processing.

In this paper we explore a relatively new area of applications for charge-coupled devices and concepts: infrared detection and imaging. A variety of infrared charge-coupled devices (IRCCD's) which have been explored or proposed fall into two main categories: monolithic and hybrid devices.

The monolithic IRCCD concept generally uses the standard CCD structure with the substrate consisting of a narrow band gap or an extrinsic semiconductor sensitive to IR radiation (refs 2,3). Other monolithic IRCCD devices being investigated combine a Schottky barrier internal photoemission sensing array in conjunction with a CCD read-out structure (ref 4). It is important to note that the extrinsic semiconductor substrate IRCCD is the only one operating in the accumulation mode (AMCCD) and using majority carrier transport, while the other monolithic IRCCD's are depletion mode devices.

*Rockwell International Corporation
Electronics Research Division
Anaheim, California, USA

**California State University
Physics Department
Long Beach, California, USA

By contrast to the monolithic IRCCD, the hybrid versions consist of the coupling of any one of various types of IR photodetectors to a silicon CCD shift register unit. In the hybrid structure, the function of detection and signal processing are performed in distinct but integratable components. The role of the silicon CCD in this case is that of a signal processor performing appropriate functions, such as multiplexing, amplification, correlation, delay-and-add, etc. The category of hybrid IRCCD's can be further subdivided into two subclasses: direct and indirect injection devices. In the former, photogenerated charge is directly injected from the detector into the CCD (ref 5), while in the latter, a buffer stage exists in between the two components. Infrared detectors used in hybrid IRCCD devices include: photovoltaic and photoconductive quantum detectors and pyroelectric detectors.

II. OPERATIONAL CONSIDERATIONS

The number of IR applications has grown tremendously over the years in all fields; military, industrial, medical, scientific, etc. (c.f. R. D. Hudson, ref 6). Existing and envisioned applications for IRCCD's fall within all of these fields. From reconaissance to surveillance to nondestructive testing and inspection to earth resource surveys, the introduction of a self-scanned solid-state IRCCD can result in an IR system with lower cost, lower package size and weight, increased lifetime and sensitivity. In this section, therefore, an attempt is made to discuss some of the common operational requirements and limitations of IRCCD's.

Due to CO_2 and water molecule absorption, infrared devices generally operate in one or more of the atmospheric transmission windows present at 2.0 - 2.5 μm, 3.5 - 4.2 μm (sometimes extended to 5.5 μm) and 8 - 14 μm (c.f. P. W. Kruse, et al, ref 7). Here a major operating difference between infrared and visible CCD's is the level of background radiation present. Assuming that the earth and most objects have an average temperature of 300°K, the spectral content of the radiation emitted is given by Planck's law (ref 7) for a blackbody of the same temperature. In the visible region of the spectrum the emitted background radiation is negligible but increases rapidly in each successive IR window from $Q_B = 10^{12}$ photons/sec-cm^2 to 10^{17} photons/sec-cm^2. The large Q_B results in increasingly shorter background charge-up or saturation time with increasing wavelength of operation, going from about 1 sec. for the 2.0 - 2.5 μm window to about 10 μsec for the 8 - 14 μm window. In addition, internally generated charge is simultaneously integrated, further reducing the saturation time (see Section IV). Thus, one limitation of practical IRCCD devices is the length of the exposure time.

Another important consideration, especially for IR thermal imaging applications, is the contrast ratio between the photon flux generated by an incremental change in background temperature and the total photon flux. For 0.1°K change (typical for IR imaging) of the average 300°K background, the contrast ratio is on the order of 10 percent in the 2.0 - 2.5 μm window and 0.1 percent in the 8 - 14 μm window. The presence of these low contrast ratios points to another practical limitation: the uniformity of IR material properties. Nonuniformity in the responsivity of the IR detectors of the same order or higher than the scene contrast ratio seriously degrades the minimum resolvable temperature and results in severe fixed pattern noise.

Finally, it should be pointed out that most IR detectors operate at reduced temperatures, pyroelectric detectors being a notable exception.

Therefore, the presence of either a passive or active cooling system is an operational requirement for IRCCD operation.

III. MONOLITHIC CCD'S

The category of monolithic IRCCD devices includes both inversion-mode devices and accumulation-mode devices, and they will be discussed in turn below. The distinguishing feature of these monolithic devices is that both the sensor and the transfer section are built up on the same semiconducting substrate. Indeed, with the exception of the Schottky barrier IRCCD, all the other monolithic IRCCD's use the same metal-insulator-semiconductor structure.

III.1 Inversion Mode Devices. The operation and structure of these devices is essentially similar to that of the Si CCD and, therefore, is based on the generation of an inversion region at the insulator-semiconductor interface where photogenerated minority carriers are collected. The bandgap of the semiconductor substrate determines the absorption peak and therefore, the useful atmospheric IR window. These narrow bandgap semiconductors are found among the binary and ternary III-V and II-VI compounds (refs 7 and 8). In this section calculations for MIS parameters essential for CCD operation are presented. These include the surface potential, thermal generation current, background current, charge storage capacity, etc. These parameters are necessary for the calculation of the storage time, the critical factor in establishing the feasibility of a practical IRCCD. The following representative semiconductors have been used in the calculations: InAs, InSb, $Hg_{1-x}Cd_xTe$. Similar calculations have been performed by Tao, et al, for PbTe and $Pb_{1-x}Sn_xTe$ (ref 9).

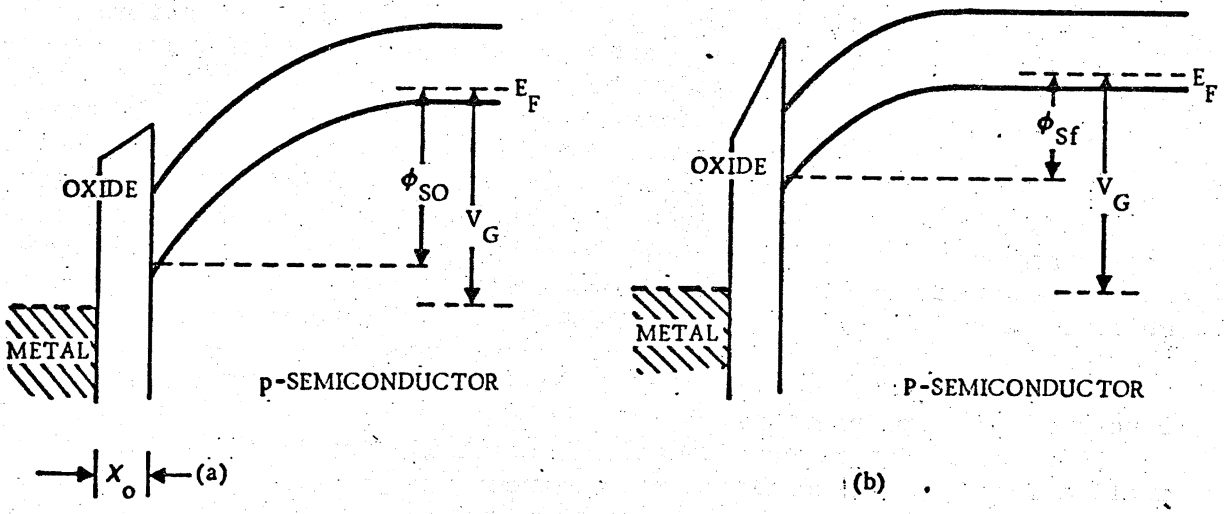

Figure 1. Energy Band Diagram for an MIS Structure
(a) Initial Conditions
(b) Steady-State

The energy band diagram for an MIS structure with a gate voltage of V_G is shown in Figure 1. The surface potential, φ_s, for the depletion region approximation of Poisson's equation is related to the gate voltage by (ref 25):

$$V_a = V_G - V_{FB} = \frac{x_o Q_{inv}}{\epsilon_o k_o} + \beta\sqrt{\varphi_s} + \varphi_s \qquad (1)$$

where $\beta = \frac{x_o}{k_o}\sqrt{\frac{2\,Nk_s}{\epsilon_o}}$, V_{FB} is the flat band voltage, x_o and k_o are the oxide thickness and relative dielectric constant, N and k_s are the semiconductor doping and dielectric constant. At t = 0 (Figure 1a) with no minority carrier charge present at the interface ($Q_{inv} = 0$), the surface potential is given by

$$\varphi_s(t=o) = \varphi_{so} = \frac{\beta^2}{4}\left(\sqrt{1 + \frac{4V_a}{\beta^2}} - 1\right)^2 \qquad (2)$$

and the depletion region its maximum width. At steady-state (Figure 1b), charge Q_{inv} has accumulated at the interface reducing the surface potential (ref 27)

$$\varphi_s(t\to\infty) = \varphi_{sf} = \frac{2kT}{q}\,\ell n\left[\frac{N}{n_i}\right] \qquad (3)$$

as well as the depletion width. The rate of change of the charge in the inversion layer is given by the summation of all current generation terms.

$$\frac{dQ_{inv}}{dt} = J_G + J_S + J_D + J_B \qquad (4)$$

$$J_G = \frac{qn_i\,x_d(t)}{2\,\tau} \qquad \text{Depletion Region Generation} \qquad (5)$$

$$J_S = \frac{qn_i S_o}{2} \qquad \text{Interface State Generation} \qquad (6)$$

$$J_D = \frac{qn_i^2\,L}{N\,\tau} \qquad \text{Bulk Generation} \qquad (7)$$

$$J_B = \eta q Q_B \qquad \text{Background Generation} \qquad (8)$$

where n_i = intrinsic carrier conc.
τ = minority carrier lifetime
$x_d(t)$ = depletion depth
S_o = surface recombination velocity
L = minority carrier diffusion length
η = quantum efficiency
Q_B = background photon flux

Since the last three terms (eq's. 6-8) are constant as a function of time they can be combined in one term

$$\frac{dQ_{inv}}{dt} = J_G + J_X \tag{9}$$

By introducing eq. 9 in eq. 1, the charge-up time for the MIS structure is obtained:

$$\tau_c = \frac{2}{\alpha}\left(\varphi_{so}^{\frac{1}{2}} - \varphi_{sf}^{\frac{1}{2}}\right) + \frac{2}{\alpha^2}\left(\frac{\alpha\beta}{2} - \gamma\right) \ell n \left(\frac{\gamma + \alpha \varphi_{so}^{\frac{1}{2}}}{\gamma + \alpha \varphi_{sf}^{\frac{1}{2}}}\right) \tag{10}$$

where

$$\alpha = \frac{x_o}{\epsilon_o k_o} \frac{qn_i}{2\tau} \sqrt{\frac{2k_s \epsilon_o}{qN}} \quad , \quad \gamma = \frac{x_o J_x}{\epsilon_o k_o} \quad .$$

In Table I, charge-up times representative of MIS structures are presented along with the pertinent material parameters. To present a balanced picture, three IR semiconductors each with a long wavelength cut off response falling in or near one of the three atmospheric windows were chosen: InAs($E_g \simeq 0.4$ eV, $\lambda_c \simeq 3.0$ μm), InSb ($E_g \simeq 0.23$ eV, $\lambda_c \simeq 5.4$ μm) and $Hg_{0.8}Cd_{0.2}Te$ ($E_g \simeq 0.09$ eV, $\lambda_c \simeq 14$ μm). SiO_2 is the insulator in all structures except for $Hg_{0.8}Cd_{0.2}Te$, where calculations for TiO_2 have also been included. The substrate is taken to be n-type in all cases, except for InSb where both n- and p-types are considered. The device is considered to be at 77°K in all cases and the field of view is taken to be 30°. Under these circumstances InAs has the largest charge-up time of approximately 0.14 seconds. Due to the relatively low photon flux in its limited spectral band from 2.0 to 2.5 μm, InAs is also the only case where the thermal charge-up time dominates. The InSb thermal charge-up time increases two orders of magnitude in going from p-type ($\tau_{th} \sim 10$ msec) to n-type ($\tau_{th} \sim 1$ sec.). However, since the background charge-up time is the dominant term here, the combined charge-up time changes only about a factor of two from 4 msec to 7 msec. Finally, for $Hg_{0.8}Cd_{0.2}Te$ MIS with an 8-14 μm spectral band the charge-up time is of the order of 10 μsec. When TiO_2 is chosen as the insulator, its higher dielectric constant ($k_o \approx 75$) increases the charge-up time for $Hg_{0.8}Cd_{0.2}Te$ to about 300 μsec. The scene contrast, defined as the ratio of the change in photon flux corresponding to a given change in scene temperature over the entire photon flux has also been calculated for the spectral bands of the three compounds. For the normal background temperature of 300°K and a $\Delta T = 0.1$°K, the contrast ratio is approximately 0.01 for the InAs case, 0.005 for InSb, and 0.001 for $Hg_{0.8}Cd_{0.2}Te$. These small contrast ratios would impose severe uniformity requirements for the fabrication of even medium scale inversion-mode monolithic IRCCD arrays, especially at the longer wavelengths. At the same time, the charge-up time also decreases rapidly with wavelength indicating that at the present time only specialized applications of this class of devices seems feasible.

III.2 Accumulation-Mode Devices. Accumulation-mode operation of an MIS structure results when the proper polarity gate voltage induces the same

Semiconductor	InAs	InSb		$Hg_{0.8}Cd_{0.2}Te$	
Substrate Doping	n	p	n	n	
E_g[(a)] eV	0.41	0.23		0.09	
λ_c[(a)] μm	3.0	5.4		14	
Spectral Band(λ_1-λ_2) μm	2.0-2.5	3.5-4.2		8-14	
Q_B[(c)]($300^\circ K, \lambda_1$-λ_2)Photons/cm^2- sec	2×10^{11}	1.5×10^{14}		5.7×10^{16}	
$\frac{\Delta Q_B}{Q_B}$[(h)]	~0.01	~0.005		~0.001	
Dielectric Constant[(e)] K_S	14.5	17		18	
Minority Carrier Lifetime τ(sec)	5×10^{-7}[(h)]	2×10^{-10}	5×10^{-8}	10^{-7}	
Intrinsic Carrier Conc. $n_i(cm^{-3})$	6.8×10^{2}[(i)]	6.4×10^{8}[(i)]	6.4×10^{8}[(i)]	2×10^{13}[(e)]	
Impurity Conc. $N(cm^{-3})$	1×10^{16}	5.5×10^{15}	5×10^{15}	7×10^{16}	
				SiO_2	TiO_2
Initial Surface Potential Φ_{so}(V)[(g)]	2.2[(b)]	2.6[(b)]	2.7[(b)]	0.64[(b)]	4.4[(j)]
Final Surface Potential Φ_{sf}(V)	0.4	0.21	0.21	0.11	0.11
Max. Inversion Region Charge Density Q_{inv} (C/cm^2)	1.2×10^{-8}	1.42×10^{-7}	1.43×10^{-7}	1.63×10^{-7}	3.2×10^{-6}
Thermal Charge-up Time τ_{th}(sec)[(f)]	~0.15	~ 9.5×10^{-3}	~1.4	~1.1×10^{-4}	~2.6×10^{-3}
Background Charge-up Time[(d)] τ_B(sec)	~3.7	~5.9×10^{-3}	~5.9×10^{-3}	~1.8×10^{-5}	~3.5×10^{-4}
Combined Charge-up Time τ_C(sec)	~0.14	~3.5×10^{-3}	~5.9×10^{-3}	~1.1×10^{-5}	~3.2×10^{-4}

(a) $T = 77^\circ K$
(b) SiO_2, 10^3 Å, $K_o = 3.9$
(c) FOV = 30°
(d) $\eta = 1$
(e) For comprehensive list of materials parameters and references see Moss et al (Ref. 26)
(f) Surface Recombination Velocity S_o = 200 cm/sec
(g) $V_G - V_{FB} = 5v$
(h) $T = 100^\circ K$ (EPIC series)
(i) Calculated
(j) TiO_2, 10^3Å, $K_o = 75$
(h) $\Delta T = 1^\circ K$

Table I
Material Properties and Charge-up Time for
Selected Metal-Insulator-IR Semiconductors

majority carrier type at the insulator-semiconductor interface as in the bulk of the semiconductor. In this manner an extrinsic (rather than a narrow bandgap intrinsic) semiconductor substrate can be used for monolithic IRCCD structures (refs 2, 3). The IR absorption peak is determined by the ionization energy of the impurity levels. For example, the extrinsic peak response gold-doped germanium (Ge:Au) occurs at 20 μm (ref 10) and Si:P peak response occurs at about 30 μm (ref 11). One can thus take advantage of the already developed silicon CCD technology and extend it to the IR region. However, to minimize the thermal generation current, temperatures below impurity freeze-out are generally required. Figure 2 shows the energy band bending in an accumulation-mode MIS structure at a subfreeze-out temperature. The bands have a linear spatial behavior through the semiconductor substrate due to the absence of space charge. The large spatial penetration of the electric field gives rise to considerable fringing fields (ref 12) which enhance the charge transfer efficiency (ref 14).

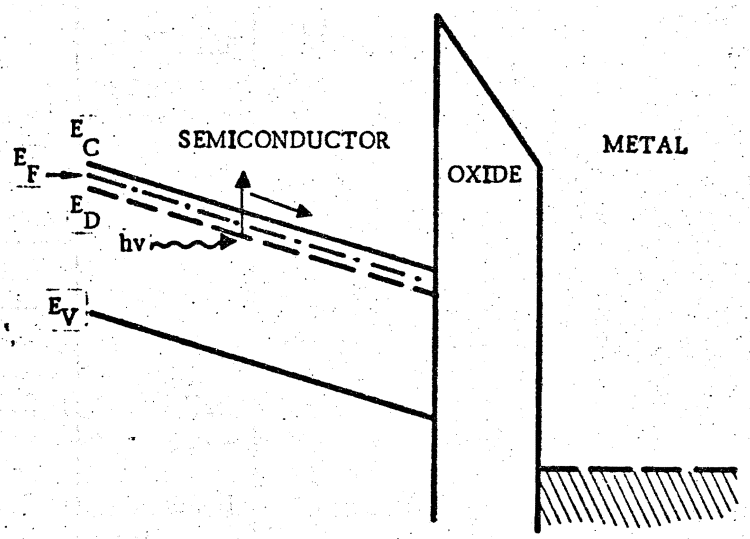

Figure 2

Energy band diagram for MIS structure biased into accumulation

Furthermore, the electric field at an accumulated semiconductor surface is much smaller than at an inverted surface because the surface potential appears across the whole thickness of the substrate, rather than only a thin depletion layer. As a consequence, the width of the accumulation layer charge packet is as much as an order of magnitude greater than an inversion layer packet. Accumulation-mode devices built and investigated by our laboratory (ref 3) have a four-phase, two-layer, overlapping-gate structure. A 64-cell, n-channel device was built on a 10^{15} cm^{-3} phosphorous-silicon substrate. The observed transfer efficiency was 0.99 per gate at a chip frequency of 25 KHz and a temperature of 4.2 °K. Calculations (ref 3) for this device indicate a charge packet depth of 300 Å. Having the charge stored at this distance from the interface reduces the importance of surface trapping states and, hence, further aids transfer efficiency.

III.3 Schottky Barrier Photoemissive Devices. Another approach to solving the nonuniformity limitations of monolithic IRCCD devices, as proposed by Sheperd and Yang (ref 4), is based on internal photoemission from metal-

semiconductor Schottky barrier arrays on a silicon substrate. The photoemission process is shown in Figure 3a: photons of energy $h\nu < E_g$ are absorbed in the metal resulting in the excitation of a hot carrier. Carriers with energy larger than the contact barrier and with sufficient momentum in that direction are emitted into the semiconductor. The depletion region set up by the application of a reverse bias voltage is diminished in size by the emitted carriers neutralizing the immobile charges at its edge (Figure 3b). The photoemitted current is, therefore, integrated by a negative charge accumulation method. The readout of the Schottky barrier detector into the CCD takes place via an MOS transfer gate which converts the initial majority carrier signal into the minority carrier transport required by the Si CCD (Figure 4).

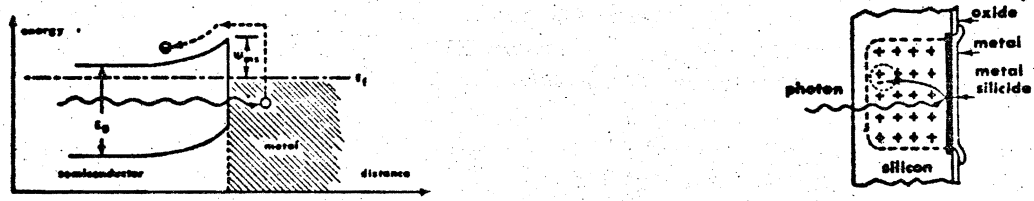

(a) Energy Band Diagram (b) Device Operation

Figure 3

Internal Photoemission in a Schottky Barrier Detector (ref 4)

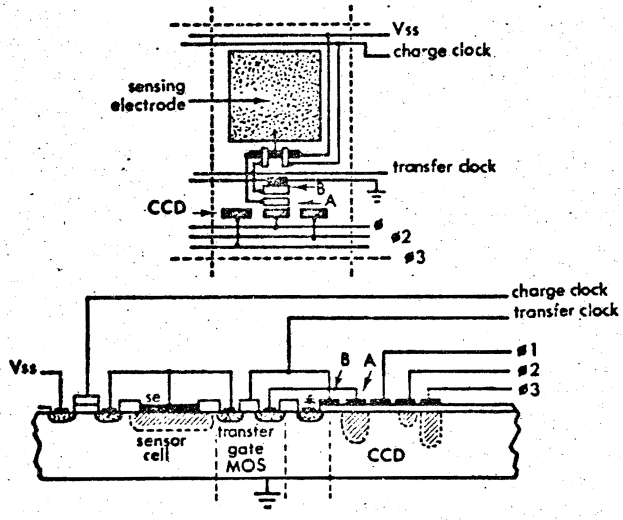

Figure 4

Schottky Barrier IRCCD Proposed by Sheperd and Yang (ref 4)

The Schottky barrier IRCCD has several main features: (a) the use of silicon and its well-known properties as the basis for the entire device; (b) the use of photodetection in a metal film, resulting in highly uniform responsivity across a typical array (approximately 1 percent, ref 4), as well as excellent reproducibility from array to array (approximately 1 per-

cent, ref 20); (c) the photoemissive yield is still relatively low, $\gamma \approx 1\%$ at $\lambda = 3.1$ μm and $T = 77^{\circ}K$ for Au-p-Si contacts (ref 21).

III.4 Other Monolithic Devices. Other monolithic IRCCD's receiving attention include: (a) Germanium-substrate CCD (ref 22). By substituting Ge for Si, one increases the intrinsic CCD response in the near infrared out to 1.85 μm. (b) Charge injection devices (ref 23, 24) use injection into the bulk for readout rather than the sequential transfer principal of CCD and, therefore, fall in a different category of devices. Infrared applications of CID's include the work of Kim (ref 24) with InSb.

IV. HYBRID IRCCD'S

Since the hybrid IRCCD involves the coupling of two already fairly well developed technologies, it has received more attention (refs 5, 15, 16, 17) to date than the monolithic concept. As mentioned in Section I, hybrid IRCCD's fall into categories: direct and indirect injection devices.

IV.1 Direct Injection Devices. In the direct injection IRCCD, the photogenerated charge is directly introduced into the CCD shift register (ref 5). Since this is in effect a DC coupled system, only those detectors with very small DC currents (e.g. photovoltaic, extrinsic detectors) can be fed into the CCD, due to the latter's limited charge handling capacity. The basic direct injection concept is illustrated in Figure 5 for an n-on-p IR photodiode and an n-channel CCD. The IR photodiode is connected in parallel to a silicon coupling diode (SCD) diffused into the same silicon substrate on which the CCD is fabricated. The first MOS gate (input) of the CCD is used to reverse-bias the IR diode and the silicon coupling diode; the TRANSFER gate is used to introduce the photocharge into the CCD through a field induced n-channel. When the φ1 gate is activated with a positive pulse, the potential well under the gate acts as a sink for the diodes and the photocurrent plus the saturation currents of the diodes will flow into the well for the duration of the φ1 pulse. When the φ2 gate is turned on and the φ1 gate is turned off, the current flow stops and the charge present is transferred on through the device.

Direct injection devices being investigated in our laboratory (ref 18) include an InSb diode array coupled to a 100-bit, p-channel CCD shift register through eight input taps. Both the detector array and the CCD have been operated at an $80^{\circ}K$ temperature. Direct injection has been observed for CCD chip frequencies up to and higher than 1 MHz.

A potential application of the direct injection hybrid IRCCD is in the serially scanned TV-compatible Forward Looking Infrared (FLIR) system (c.f. A. F. Milton, ref 19). The serially scanned FLIR uses a linear array of detectors raster-scanned across the scene, the scan direction being parallel to the array. Since each detector in turn scans the entire field of view, the dwell time per resolution element is approximately 150 ns. The amount of charge generated during this dwell time in even an 8 - 14 μm IR detector by a $300^{\circ}K$ blackbody is well within the charge handling capacity of a typical CCD shift register. By processing the outputs of the detectors through a delay-and-add operation, the components of the signals corresponding to the same resolution element are summed linearly. Because the noise contribution of each detector is independent and thus uncorrelated, the total noise is obtained by a root mean square summation. For an array of m detectors, the delay-and-add operation could, therefore, result in a maximum improvement of $\sqrt{m}$ (in the detector noise limited case) in the

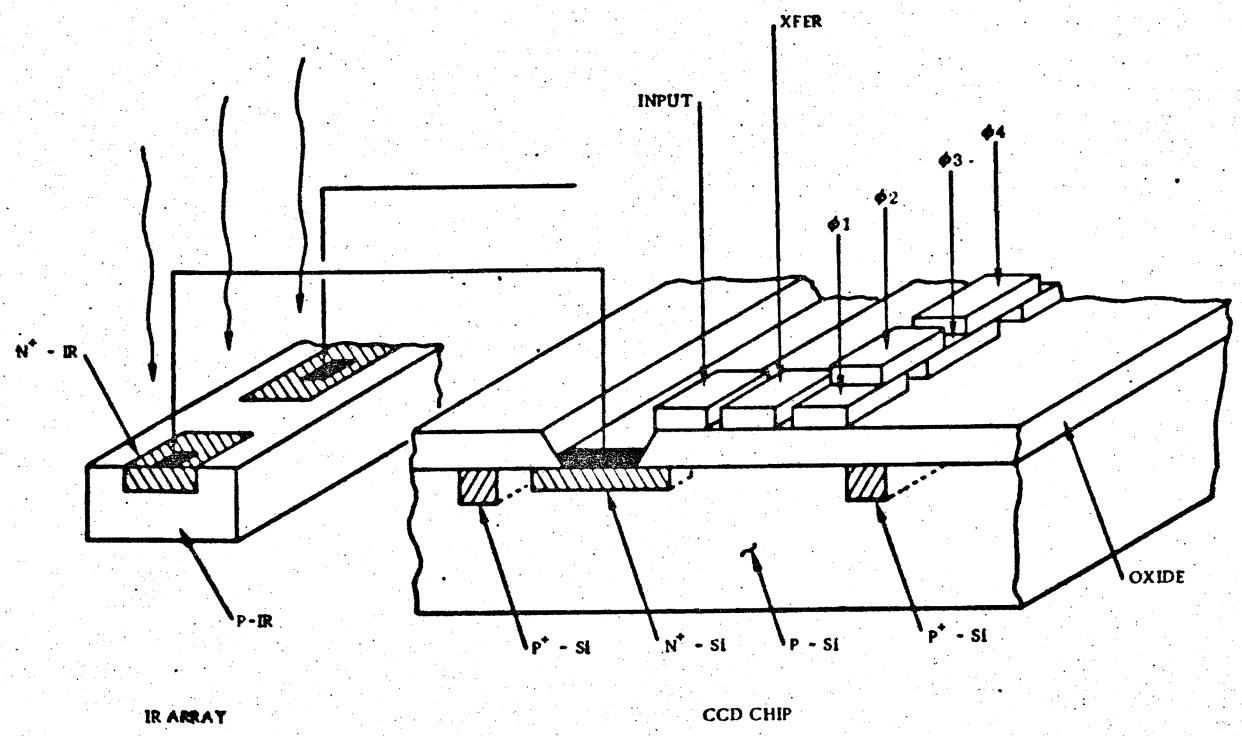

(a) Coupling Concept

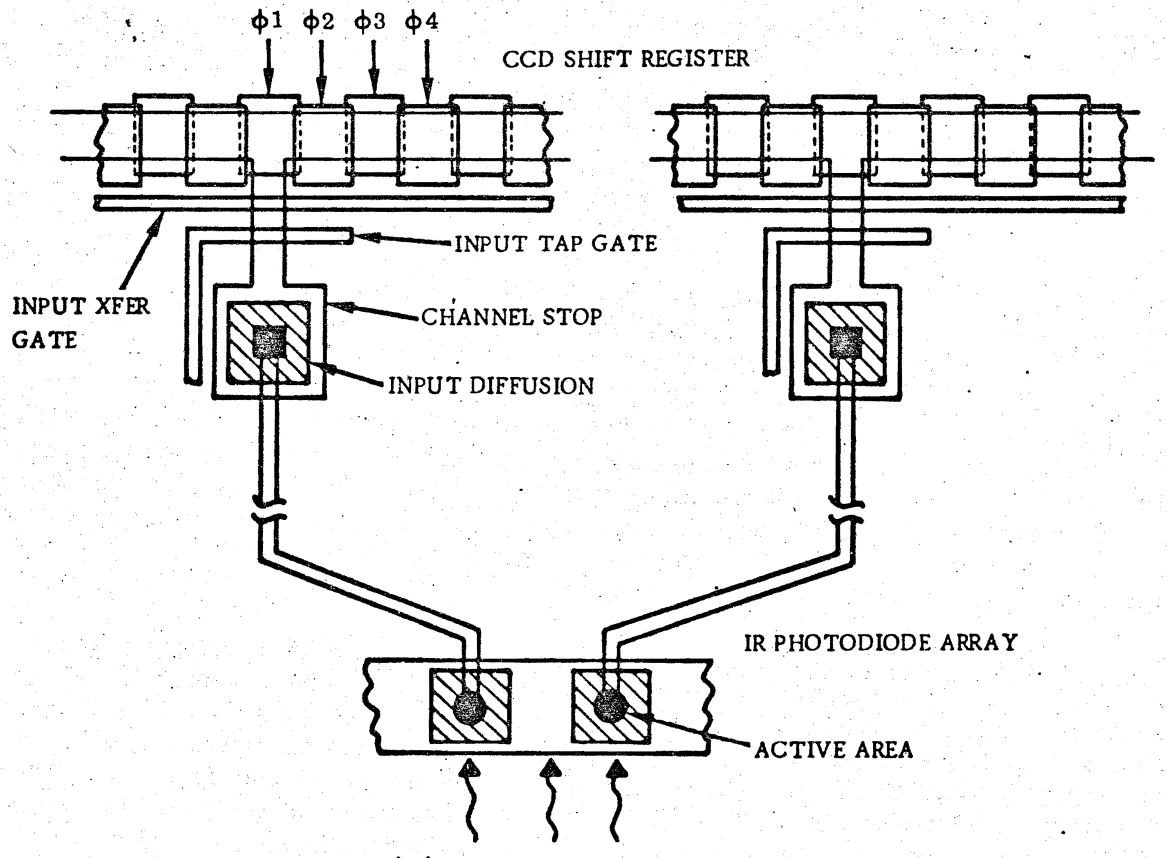

(b) Array Layout

Figure 5. Direct Injection Hybrid IRCCD

signal-to-noise ratio (SNR) of the entire array over that of a individual detector. The upper limit of m and, therefore, of the maximum SNR improvement achievable is set by the total detector array signal versus the CCD charge capacity. The operation of the entire array appears at the CCD output essentially as one detector. This results in no fixed pattern noise, lowered detector response uniformity requirements as well as built-in redundancy. These features together with the potential $\sqrt{m}$ improvement in SNR help circumvent the problems posed by the high background and low contrast ratio present in thermal imaging systems at infrared wavelengths.

A signal-to-noise ratio analysis for a direct injection hybrid IRCCD operated in the delay-and-add mode was developed by Steckl and Koehler (ref 5). For a typical application consisting of an array of nine 12μm (Hg,Cd)Te photodiodes receiving an incident flux of 3×10^{17} photons/cm^2-s ($T_B = 300^oK$, FOV = 90^o), they calculate a signal-to-noise ratio of 500, a dynamic range of 300 and a noise equivalent change in temperature of 0.1^oK.

IV.2 Indirect Injection Devices. Indirect injection hybrid IRCCD's use a buffer stage between the photodetection stage and the CCD shift register. The buffer stage can vary from one on-chip MOSFET to a number of off-chip amplifiers. It is the simplest version that is more appealing in its simplicity and ease of integration. Two indirect injection devices, one using pyroelectric detectors and the other photoconductive twin films, are discussed below.

IV.2.1 Indirect Injection: Pyroelectric Detectors. Pyroelectric materials owe their photodetection property to a temperature dependent polarization (for a review of pyroelectric detectors, see E. H. Putley, Ref 28). The main advantages of pyroelectric detectors are inexpensive detector materials and room temperature operation. Unfortunately, the sensitivity of pyroelectric detectors is considerably lower than that of quantum detectors.

Detection of the thermally-induced electric polarization of the pyroelectric is accomplished by making the pyroelectric the dielectric of a capacitor. Two methods of introducing the pyroelectric signal into a CCD are (i) connecting the capacitor to an on-chip MOSFET, as mentioned above, or (ii) fabricating a pyroelectric film between the MOSFET channel and the gate metal (viz., in series with the gate). Both methods are essentially the same, the latter requiring more sophisticated processing but resulting in a more compact structure. A potential problem for pyroelectric hybrid IRCCD array deals with thermal isolation. Good thermal isolation between closely spaced elements is required to prevent thermal loading by the substrate as well as inter-element crosstalk.

IV.2.2 Indirect Injection: Photoconductive Films. A technique which can be utilized with any photoconducting film which can be deposited on silicon dioxide without inducing fast states (or interface traps) at the silicon-silicon dioxide interface is described. The photoconductive film is used to directly influence the inversion of the channel of the input MOSFET. The degree of inversion, in turn, controls the rate of charge flow into the CCD. The photoconductive gate device is shown in Figure 6. The advantage of this method is that the photoconductive film can be deposited by a variety of techniques after all the silicon MOS CCD process steps have been performed.

Operation of the device is described by the following sequence of steps:

1. A voltage sufficient to deeply invert the oxide is applied to the R bias line.

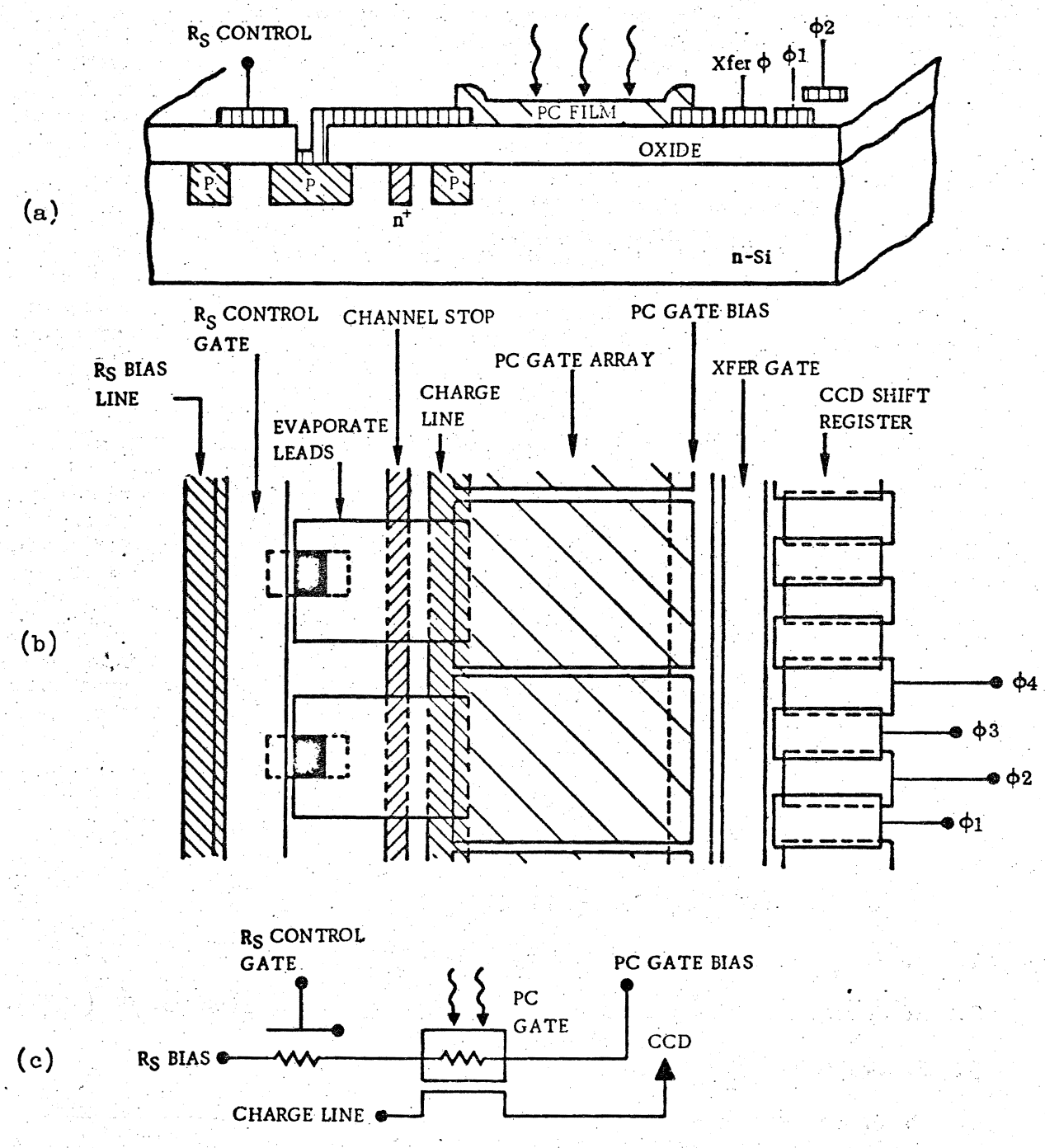

Figure 6

Indirect Injection: Photoconductive Thin-Film Hybrid IRCCD
(a) Device Cross-section
(b) Two-dimensional Layout
(c) Equivalent Circuit

2. A voltage is applied to the R_s control gate which provides resistance in series with the photoconductive gate.

3. The PC gate bias is set just above the threshold value of voltage for this gate. This results in the transfer of maximum charge in the absence of optical input signal, providing blooming protection.

4. Incident photons cause the resistance of the PC films to decrease accordingly. This causes a drop in the voltage across each PC film inversely proportional to the local density of incident photons.

5. The charge passing into the CCD is now a function of the illumination level falling upon the PC film. The response of the device to optical signal transients is governed by the ability of the biasing resistor to discharge the PC gate capacitance.

This device scheme, while hybrid and indirect, provides a straightforward and relatively easily fabricated method of IRCCD imaging array.

V. CONCLUSIONS

A review of applications of charge-coupled devices for infrared detection and imaging has been presented. It is obvious even at this fairly early stage that a large number of avenues to the development of IRCCD's exist. Indeed, no one approach seems to be versatile enough in the broad sense of the word to be developed as a building block for a wide range of applications. Consequently, the research and development of IRCCD's in the immediate future will in all probability continue along many paths, each closely tied to a specific end-use function. In this context operating parameters and requirements (sensitivity, cooling, size, present and future costs, to name only a few) of the particular system in which the IRCCD is to be integrated become the key selection factors.

ACKNOWLEDGEMENT

The authors would like to acknowledge useful discussion and encouragement of R. A. Gudmundsen.

REFERENCES

1. W. S. Boyle and G. E. Smith, Bell Sys. Tech. J. 49, 587 (1970).

2. R. Keyes, IRIS Specialty Meeting on IR Detectors, El Toro, CA (1974).

3. R. D. Nelson, to be published.

4. F. D. Sheperd and A. C. Yang, Technical Digest--International Elec. Devices Meeting, Washington, D. C. (1973) p. 310.

5. A. J. Steckl and T. Koehler, Proc. CCD Applications Conf., San Diego, CA (1973) p. 247.

6. R. D. Hudson, Infrared System Engineering (John Wiley & Sons, NY, 1969).

7. P. W. Kruse, L. D. McGlauchlin and R. B. McQuistan, Elements of Infrared Technology (John Wiley & Sons, NY, 1962).

8. R. K. Willardson and A. C. Beer, Eds, Semiconductors and Semimetals, Vol. 5 (Academic Press, NY, 1970)

9. T. F. Tao, J. R. Ellis, L. Kost and A. Doshier, Proc. CCD Applications Conf., San Diego, CA (1973) p. 259.

10. Lasser, Cholet and Wurst, J. Opt. Soc. Amer. 48, 468 (1958)

11. R. A. Soref, J. Appl. Phys. 38, 5201 (1967)

12. J. E. Carnes and W. F. Kosonocky, IEEE J. Solid-State Circuits 6, 322 (1971).

13. C. N. Berglund and K. K. Thornber, IEEE J. Solid-State Circuits 8, 108 (1973).

14. L. G. Heller and H. S. Lee, IEEE J. Solid-State Circuits 8, 116 (1973).

15. D. M. Erb and K. Nummedal, Proc. CCD Applications Conf., San Diego, CA, (1973), p. 157.

16. D. E. French, M. Y. Pines, F. J. Renda, P. S. Chia, J. B. Balon and A. H. Lockwood, Proc. 22nd National IRIS Conf., Dayton OH (1974).

17. J. C. Fraser, D. H. Alexander, R. M. Finnila and S. C. Su, Proc. 22nd National IRIS Conf. Dayton, OH (1974).

18. A. J. Steckl, to be published (Internal Letter No. 74-520-011-100, Rockwell International, June 1974).

19. A. F. Milton, IRIS Detector Specialty Meeting, Washington, D. C. (1973).

20. F. D. Sheperd, personal communication.

21. J. Cohen, J. Vilms and R. Archer, Air Force Cambridge Laboratory Report Nos. AFCRL-68-0651 and AFCRL-69-0287.

22. D. K. Schroder, Proc. 22nd National IRIS Conf., Dayton, OH (1974).

23. G. J. Michon and H. K. Burke, Digest IEEE International Solid-State Circuits Conf., Philadelphia, PA (1973) p. 138.

24. J. C. Kim, Digest International Elec. Devices Meeting, Washington, D. C., (1973) p. 419.

25. G. F. Amelio, W. J. Bertram and M. F. Tompsett, IEEE Trans. Elec. Devices, ED-18, p. 986 (1971).

26. T. S. Moss, G. J. Burrell, B. Ellis, Semiconductor Optoelectronics (J. Wiley & Sons, 1973).

27. S. M. Sze, Physics of Semiconductors Devices, (J. Wiley & Sons, 1969).

28. E. H. Putley, p. 259 in Ref. 8.